Perylene diimide derivative dispersed in LDH as a new efficient red-emitting phosphor for LED applications

Yixuan Guo, Damien Boyer, Federico Cisnetti, Anthony Barros, François Reveret, Yongjun Feng, Geneviève Chadeyron, Fabrice Leroux

Perylene diimide derivative dispersed in LDH as a new efficient red-emitting phosphor for LED applications

Yixuan Guo,[1,2] Damien Boyer,[1*] Federico Cisnetti,[1] Anthony Barros,[1] François Reveret,[1] Yongjun Feng,[2] Geneviève Chadeyron,[1] Fabrice Leroux[1*]

[1] Université Clermont Auvergne, Clermont Auvergne INP, CNRS, ICCF, F-63000 Clermont–Ferrand, France.

[2] State Key Laboratory of Chemical Resource Engineering, Beijing Engineering Center for Hierarchical Catalysts, Beijing University of Chemical Technology, No. 15 Beisanhuan East Road, Beijing 100029, China.

E-mail : fabrice.leroux@uca.fr, damien.boyer@sigma-clermont.fr

Abstract

Perylene diimide-based dyes substituted by four sulfonate groups at their *bay* position are known to be extremely sensitive to their mutual π – π intermolecular interaction. They do not emit fluorescence in solid state. When co-hosted in LDH with a surfactant in extremely small quantities, an absolute photoluminescence quantum yield (PL QY_{abs}) of about 35 % is reached upon blue excitation at 465 nm for a dye content as low as 0.1 % of the total interleaved anions and yet revealing the presence of excimers. When this material is dispersed in silicone, the emission spectrum exhibits a blue shift compared to the hybrid assembly. A saturated red color with PL QY_{abs} as high as 50% is obtained. when this red-emitting film is combined with a YAG/ Ce silicone film and a blue LED chip emitting at 465 nm, warm white light (T = 3366 K) with a high color rendering index of 91.4 is produced. Finally, the phosphors hosted in LDH are photo-stable even when dispersed in a silicone matrix, with emission properties that do not suffer any decrease in intensity under combined thermal and photonic stresses, thus opening up real possibilities for applications in LED technology.

Keywords

Tetra Sulfonated Perylene diimide, organic fluorophores, LDH composite, LED display, red-emitting phosphor

1. Introduction

Most of the LED devices available on the market contain rare-earth elements (REEs), which are used in the composition of phosphors to produce white light. However, supply constraints, including rising prices and environmental concerns over mining and refining processes, are of concern for manufacturers. To overcome these issues, the development of rare-earth-free phosphors is challenging. [1] Currently, the majority of LED lighting devices comprise a blue chip (450-465 nm) combined with a yellow-emitting phosphor, the familiar YAG:Ce^{3+}, and a red-emitting one. The latter makes it possible to extend the spectral coverage over the entire visible range and thus to achieve white-light emitting diodes (WLEDs) with a warmer hue and a color rendering index (CRI) suitable for use in the field of consumer lighting, where values above 90 are required. Numerous studies addressing the synthesis of red phosphors compatible with blue chips have been reported in the literature. [2-6] Eu^{2+} doped sulfides and nitrides are generally used as red-emitting phosphors in commercial WLEDs, although most of them have several drawbacks, including poor thermal stability, water sensitivity or high cost, in addition to containing REEs. [7,8] Another commercial and efficient red-emitting phosphor is K_2SiF_6:Mn^{4+}, but its synthesis process involves the use of a highly toxic starting material, HF. [8,9] Thus, developing red-emitting rare-earth-free phosphors that can be efficiently excited by blue photons can be considered as a real challenge, in particular when an environmentally-friendly process is sought. To fulfill such requirements, polycyclic aromatic hydrocarbons with extended π-conjugated backbones, and in particular perylene diimide-based organic molecules (PDI), are promising candidates since they have outstanding optical properties and they can exhibit strong emissions at different wavelengths, depending on their backbone substitution. [10-14] For instance, a red-emitting derivative is obtained for tetrasulfonate-substituted PDI at the *bay* positions, [15] hereafter named TSP. The latter gives rise to red fluorescence centered at 619 nm, with a high quantum yield of about 60% measured in an aqueous medium. However, as commonly observed, these organic compounds do not emit light in solid state due to a

quenching effect, the so-called aggregation-caused quenching (ACQ) phenomenon, since the molecules aggregate themselves through π – π intermolecular stacking. [16,17] In the case of TSP, the substitution on the phenyl ring results in a loss of planarity for the aromatic perylene scaffolds; this has the effect of separating the monomers from one another, but not enough to avoid ACQ.

To protect these fascinating PDI π-scaffolds from optical quenching in their solid state, two main routes are reported. The first consists in positioning substituents onto the PDI backbone, either at the imide or *bay* positions. [18-20] Cumbersome substituents such as voluminous phenoxy groups attached at the *bay* positions entirely wrap the dye core, thus preventing the deleterious intermolecular π – π interaction. [21] Fully "jacketed" PDI leads to a chromophore-to-chromophore distance of 1.57 nm and a photoluminescence quantum yield (PL QY) in solid state of up to 60%. Indeed, direct π – π contact < 0.4 nm until an intermolecular distance of about 1 nm provokes rapid fluorescence quenching. [22] As far as PDI chemical substitution is concerned, the *bay* functionalization is preferred to the imide counterpart. Indeed, a long alkyl chain at the imide position does not avoid substantial π – π interaction; the derivative molecules stack themselves at a distance as close as 0.36 nm. [23]

Another possibility to move molecules away from each other is to disperse them in a solid medium by mixing them with other molecules. For instance, a straightforward approach to wrapping PDI is to use soft matter such as dendrimers. [24,25] Other studies report mixing a multilayer alternated assembly using poly(sodium 4-styrene sulfonate) or directly with surfactant micelles such as hexadecyltrimethylammonium bromide (CTAB). [26,27]

Beside these physical mixtures, an elegant method to shield PDI π – π intermolecular interaction is to use them as a linker to engineer a MOF structure or to confine them in a layered host structure. The formation of a 3D structure prohibits close π – π contact. [28-30] Pioneering works showed the interest of layered double hydroxide (LDH) in hosting optically active molecules, [31-33] but they failed to present high PL QY, since the phosphor anions are highly packed in the interlayer space, presenting a J-type herringbone accommodation that reduces as well as shifts the luminescence contribution. To overcome this issue for fluorophores like tris(8-hydroxyquinoline-5-sulfonate), [34] indocyanine green, [35] the quantity of phosphors is

reduced by co-intercalating them with a surfactant, [36] and LDH hosting is revisited by adapting the relative quantity of interleaved phosphors.

The LDH structure is described by brucite $Mg(OH)_2$, in which the substitution of divalent by trivalent cations creates an excess positive intralayer charge compensated by interleaved anions, as indicated by the formula $M^{2+}_{1-x}M^{3+}_{x}(OH)_2$ $A^{n-}_{x/n}\cdot H_2O$ [37-40] Anions to be interleaved during co-precipitation should be water-soluble, such as TSP.

In this work, relying upon previous studies, [34,41,42] TSP and sodium dodecyl sulfonate (SDS) molecules were co-intercalated in the interlayer region of hydrotalcite by co-precipitation. SDS spacers expand the LDH gallery and disperse TSP guests in order to target desired red-emitting layered solid-state supramolecular material. After a structural analysis of the different samples, their optical properties were investigated. Surprisingly, only around one tenth of one percent of luminescent molecules was sufficient to endow the solid powder with a red fluorescence characterized by a high PL QY, which remained the case when dispersed into a silicone film for LED embarked display. Furthermore, a WLED prototype was created by combining this red-emitting film with a yellow one containing YAG:Ce^{3+} and a blue chip (465 nm), and its photometric parameters (chromaticity coordinates, correlated color temperature (CCT) and color rendering index (CRI)) were measured. Finally, a stability study of the optical properties was performed under photonic stress in order to assess the reliability of this efficient red-emitting composite film for commercial LED lighting applications.

2. Results and discussion

A perylene derivative red-emitting candidate was prepared straightforwardly from perylene diimide after a sequence of classical organic transformations (see experimental section). In short, ortho-alkyl-substituted aromatic groups were introduced at the terminal positions of PTCD-4Cl through an imidization reaction. Next, four phenoxy groups were introduced at the bay positions of PDI, leading to a bathochromic shift (electron-donating effect) and enhanced solubility based on the anti-aggregation effect. Finally, four sulfonic acid groups were tethered to the phenoxy groups to yield a compound which was easily soluble in aqueous basic medium after deprotonation. [43,44] Characterized by ^{1}H NMR (Figure

S1), the tetra-sulfonated perylene based dye (TSP) is indeed highly water-soluble (> 200 g/L) making its intercalation straightforward during an aqueous co-precipitation. [45,46] Based on its structure, shown in Figure 10b, TSP should easily accommodate a LDH host sheet via electrostatic interaction through its four sulfonate groups.

Relying upon previous studies, TSP and SDS were here co-intercalated into the interlayer region of LDH by co-precipitation. It is noteworthy that the supernatant is colorless, and its characterization by UV-vis spectroscopy (Figure S2) does not show the presence of TSP, indicating that the amount of TSP used was entirely embedded in the LDH structure.

A series of TSP_x-LDH samples was synthesized by tuning the feeding molar ratio of the organic compound from 0.005 to 1%. PXRD patterns of PDI derivative, DS-LDH and TSP_x-LDH are presented in Figures 1a. All the LDH samples exhibit a series of well-defined Bragg diffraction peaks characteristic of LDH materials, e.g. (003), (006), (009), and (110) marked in the graph. The (00ℓ) interplanar spacings show strict harmonicity ($d_{(003)} = 2d_{(006)} = 3d_{(009)}$) indicating orderly stacking. The basal *d*-spacing of DS-LDH of about 2.49 nm, calculated from the values corresponding to three harmonic peaks ($c = (d_{(003)} + 2d_{(006)} + 3d_{(009)})/3$), agrees with the literature. For the series of TSP_x-LDH samples, the size of the interlayer space is constant regardless of TSP dye content. The thickness of the brucite-like layer is 0.48 nm; thus the interlayer spacing is about 2.01 nm, smaller than the length of TSP anions (2.53 nm). A slight tilt is possible to explain this apparent discrepancy, as has been reported for other perylenes. [32] Overall, this implies an intercalation of organic PDI derivatives with no significant effect on the structural coherence length of DS-LDH because of their relatively small quantity; the basal spacing is completely imposed by the surfactant. The phosphor TSP diffracts in its solid state, and three large diffraction peaks are identified in Figure 1b. Their positions shed light on the molecule π-stacking, with an intermolecular spacing value of 1.2 nm, in agreement with the literature. [21] As mentioned before, this value is not enough to avoid luminescence quenching, TSP is deep maroon in color, indicating the efficiency of π - π interaction (Fig. 1c). [10] Interestingly, TSP stacking disappears when the phosphor is hosted in LDH, and the color of the associated hybrid turns intense pink.

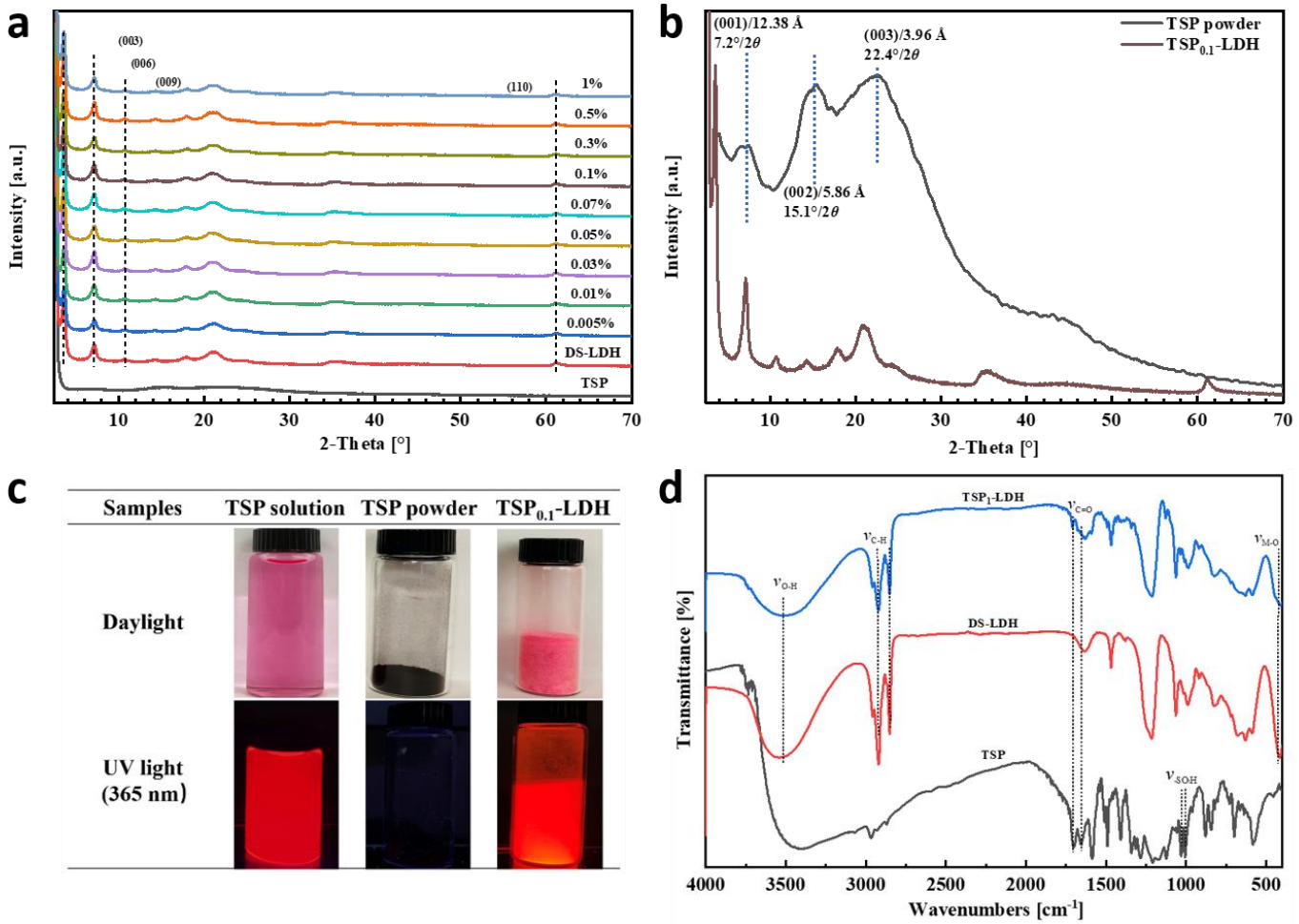

Figure 1. (a) PXRD patterns of TSP, DS-LDH, TSP_x-LDH (x varying between 0.005 and 1) samples; (b) zoom on XRD patterns of TSP powder (grey XRD pattern) and TSP_x-LDH powder (x = 0.1% -brown XRD pattern); (c) photographs of TSP aqueous solution (10^{-5} mol/L), TSP powder and $TSP_{0.1}$-LDH under daylight and 365 nm UV light; (d) FT-IR spectra of TSP, DS-LDH, and TSP_1-LDH.

As shown in Figure 1d, DS-LDH and TSP_1-LDH present characteristic LDH structure IR absorption bands: ca. 3500 cm^{-1} for the O-H stretching vibration, ca. 1637 cm^{-1} for the H-O-H deformation vibration of interlayer water, and ca. 426 cm^{-1} for the lattice vibration (Mg-O and Al-O) from LDH layers. Furthermore, the distinctive absorption peaks of DS anions (2923 and 2845 cm^{-1} for C-H stretching vibration, 1220 and 1065 cm^{-1} for $-SO_3^-$ group) are observed in the LDH samples. Notably, TSP_1-LDH shows other weak absorption signals at 1658 and 1703 cm^{-1} attributed to C=O of TSP guests. These results confirm that SDS and TSP_1 molecules are successfully co-intercalated into the LDH interlayers.

Figure 2 presents the structure of SDS and TSP co-intercalated LDH matrices, in which the SDS spacer is devoted to expanding the LDH gallery as well as further dispersing TSP guests in the interlayer space.

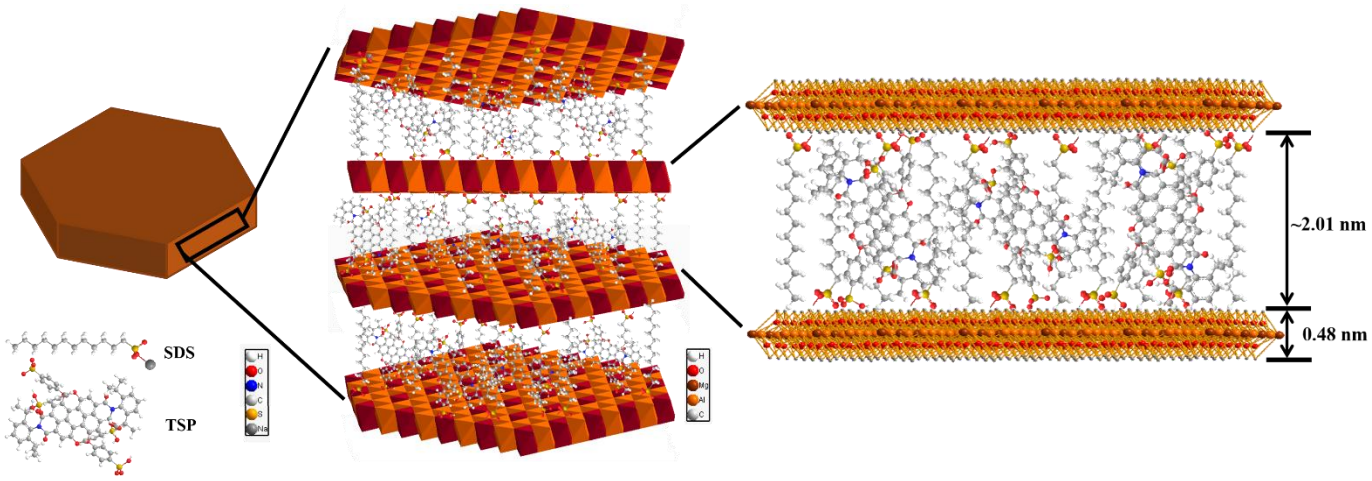

Figure 2. Scheme of SDS and TSP co-intercalated LDH composite structure.

SEM image recorded from TSD-LDH sample exhibits the common morphology expected for LDH platelets (Figure S3).

Normalized UV-vis absorption and emission spectra of $TSP_{0.1}$-LDH powder are recorded in solid state, compared with those of TSP in aqueous solution (10^{-5} mol/L), which can elucidate the interaction between the aromatic cores under various states (Figure 3). For PDI molecules, the electronic absorption has a pronounced coupling to the vibronic features corresponding to $v = 0 \rightarrow v' = 0$, 1, and 2 transitions, where v and v' are quantum vibrational numbers of the ground and excited states, respectively. [47] TSP solution exhibits three absorptions in the range of 450-650 nm: the longest wavelength band (0→0 transition, λ_{max} = 570 nm) is the most intense band with an obvious shoulder at shorter wavelengths (0→1 transition, λ_{max} = 530 nm) and a peak near 453 nm (0→2 transition). [48] Comparatively, most of the typical absorption bands of TSP free tumbling molecules show similar features when immobilized in the LDH host. In detail, the absorption contribution of 0→1 at around 530 nm and the 0→2 transition at 453 nm increases against that of the 0→0 transition, suggesting a partial aggregation of the interleaved phosphors. Of particular interest is the fact that the vibronic bands in the range of 500–650 nm are slightly broader than in solution. This is the result of a combination of π – π interactions between face-to-face stacked chromophores and interactions of anionic perylene dyes with LDH layers. [49,50] Notably, the emission spectrum (EM) of TSP solution displays a broad and asymmetric band in the range of 600–750 nm, where a maximum at around 624 nm and a large shoulder at around 678 nm are assigned to monomers and aggregates, respectively. LDH solid has a similar emission spectrum, and monomer and excimer emissions emerge at 621 and 650 nm, respectively. The

contribution of the excimers is significantly higher than that of dye solution. The hypsochromic shift (20 nm) of the shoulder band might be caused by the host-guest interaction and dilute medium DS anions that prevent the TSP molecular π-stacking effect. [51,52] Quantitatively, TSP content in the entire LDH powder is calculated to be about 10^{-3} mol/L (Figure S2). At a similar concentration of 10^{-3} mol/L, the fluorescence performance of TSP in aqueous solution decreases drastically due to multiple aggregations, as evidenced in a normalized UV adsorption spectrum (Figure S4). This further convinced us of the superior confinement and dispersing effect supplied by LDH layers and co-intercalated DS guests. As seen in Figure 1c and even with the naked eye, $TSP_{0.1}$-LDH exhibits a strong red emission, brighter than the dye solution (10^{-5} mol/L), while dye powder does not display fluorescence at all because of the aggregation-caused quenching (ACQ) effect. The very good fluorescence performance confirms that the LDH system appropriately accommodates organic dyes, limiting their guest-guest mutual interactions and disrupting their π – π packing, formed in an orderly assembly in solid state.

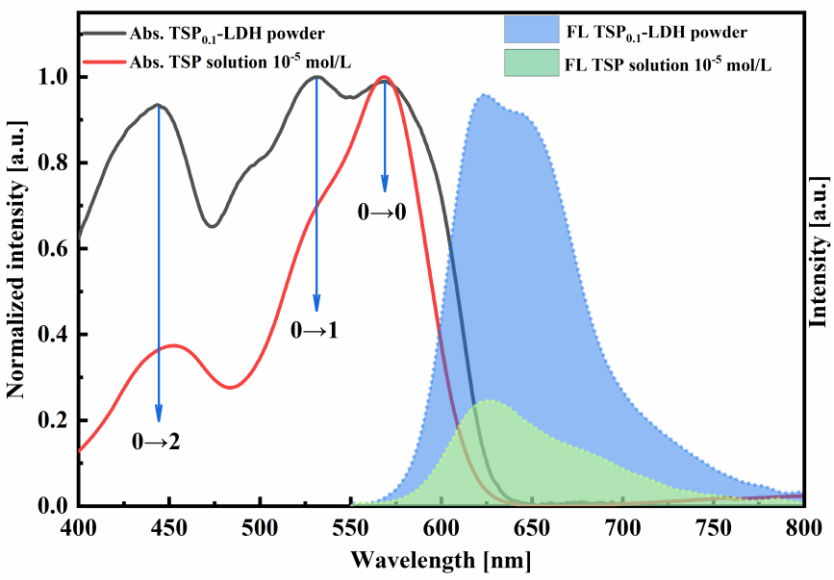

Figure 3. UV-vis absorption and emission spectra of TSP aqueous solution (10^{-5} mol/L) and $TSP_{0.1}$-LDH powder.

The variations in PL QY_{abs} of the TSP_x-LDH samples as a function of excitation wavelengths are shown in Figure 4a. Three significant excitation wavelengths are highlighted by dotted lines: 385 nm, 450 nm and 465 nm, relative to the commercial UV and blue excitation sources respectively. In the 250-550 nm excitation range, the PL QY_{abs} versus λ_{exc} curves for the studied series show a similar profile. TSP concentration- and excitation wavelength-dependent PL QY_{abs} values ranging from about 10 to 50 % are recorded. Focusing on the behavior of the samples excited at 465 nm (Figure 4b),

corresponding to excitation by a commercial blue chip, it can be noticed that absorbance increases continuously as the TSP concentration rises in our materials, and reaches a plateau for the highest TSP concentrations. Concomitantly, the internal quantum yield drops drastically as soon as the TSP concentration exceeds a critical value that can be associated with the formation of aggregates. The best-performing sample is the one that leads to the highest absolute photoluminescence quantum yield (PL QY_{abs}) i.e. the $TSP_{0.001}$-LDH with a PL QY_{abs} value of 45% and 35% for excitation at 450 nm and 465 nm, respectively. The PL $QY_{abs,}$ which is the product of the absorption coefficient, and the PL QY_{int} result from the best compromise between these two parameters.

Figure 4c shows the emission spectra of the series, recorded under excitation at 465 nm, as a function of TSP content. All samples mainly show two fluorescence peaks covering a wide range of wavelengths from 550-770 nm: the peak at shorter wavelengths can be attributed to single molecules, while the longer wavelength contribution can be associated with excimer forms. The relative intensity of the short-wavelength emission band increases with the concentration of TSP and reaches a maximum value for x = 0.1%. Concurrently, the contribution at longer wavelengths increases progressively with TSP concentration. It should also be noted that the ratio between the two emission bands is modified as TSP concentration increases, suggesting a transition between two states, one predominant for low TSP concentrations where the molecules are well isolated and the second, which becomes predominant as the TSP concentration increases, favoring the formation of J-type aggregated forms. [53,54] The variations in monomer/excimer contributions as a function of TSP content in the emission spectra are clearly demonstrated in Figure 4d. The contribution of the monomer and excimer forms, determined after the deconvolution of the emission bands and the integration of the area under the curve of each contribution, as a function of the TSP concentration in the LDH matrix clearly shows that the 0.3-LDH TSP sample is the one which corresponds to an equilibrium between the monomer and excimer forms. Indeed, above this value, the emission spectrum is dominated by the contribution of the aggregated forms, whereas below this value, the emission of the TSP is well isolated in the interstitial space of the LDH matrix and the contribution of the monomeric forms predominates. Based on variations in the dominant emission peak, LDH matrixes display a clear bathochromic shift in the range from 614 to 655 nm, which is

known to be caused by an increase in the π – π interaction resulting from the co-facially stacked assembly of PDI interleaved molecules. [32] Since some of the intercalated TSP molecules in the LDH galleries are inclined to π-stack (parallel stacking) at a certain content level, the optimal PL value is found with a low concentration (0.1%) of TSP molecules in the LDH inter-lamellar space. Remarkably, since PL properties are not usually met in solid state, it is here even more intense than the corresponding dye solution with an identical concentration (Figure S5). This means that in spite of the molecular tumbling provided by Brownian motion, the synergistic π – π stacking acts as a driving force in solution to self-aggregate TSP phosphors, while the anchoring effect provided by host sheet, as well as the high dispersion provided by the surfactants, is more efficient in displaying excellent PL performances in the solid state. To our knowledge, such low dye contents have not yet been scrutinized in the literature.

To evaluate TSP_x-LDH powders for LED applications, the optimized composition $TSP_{0.1}$-LDH is encapsulated into silicone to fabricate an optical-functional flexible composite film. Films named after Si-LPH with a filler loading from 20 to 40 wt. % and a thickness of 120 ± 5 µm were prepared according to the procedure described in the experimental section. The XRD pattern of Si-LPH (40 wt.%) film shows the typical Bragg reflection peaks of LDH platelets (Figure S6).

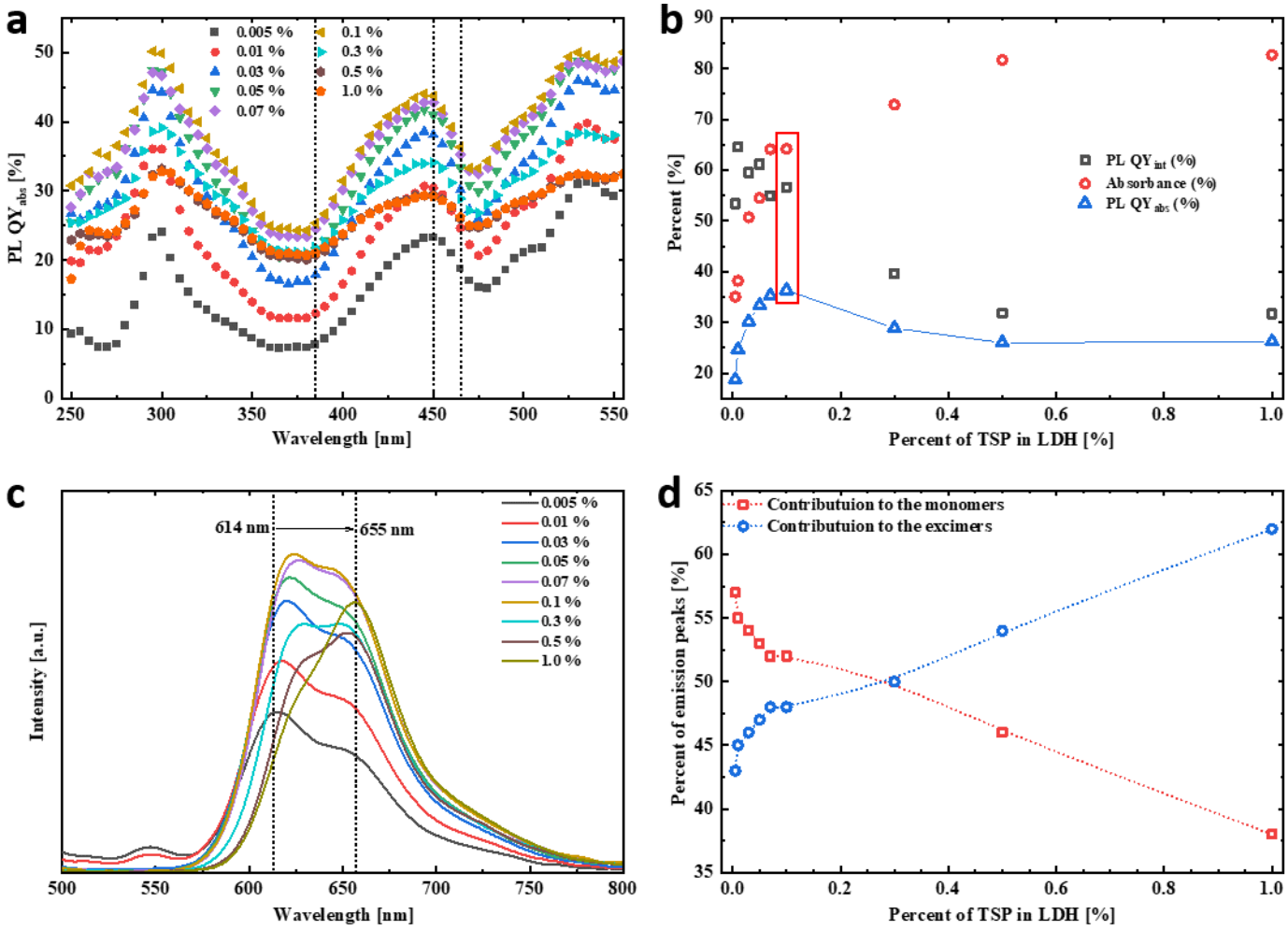

Figure 4. Optimization of the phosphor percentage: (a) variations in PL QY_{abs} of TSP_x-LDH samples as a function of excitation wavelengths. The dotted lines correspond to the excitation wavelengths of commercial LEDs; (b) PL QY_{int}, Absorbance, and PL QY_{abs} as a function of the TSP percentage (x%) in LDH at 465 nm excitation; (c) emission spectra of TSP_x-LDH with excitation at 465 nm; (d) variations in the contributions to monomers and excimers in the emission spectra as a function of the contents of TSP in LDH under 465 nm excitation.

As illustrated by SEM image (Figure S7a), a homogeneous silicone composite film was prepared with loading as high as 40 wt. % of $TSP_{0.1}$-LDH fillers; the uniform dispersion of LDH particles is clearly identified by EDX analysis (Figure S7b and S7c). Such a loading rate corresponds to a masterbatch which is usually difficult to achieve, thus underlining the excellent compatibility of the organo-modified LDH with the dispersive silicone. The optical performance of Si-LPH films was compared to that of $TSP_{0.1}$-LDH powder (Figure 5). The PL QY_{abs} curve between LDH powder and Si-LPH film (40 wt.%) shows similar features but with higher values, close to 50% on 450 nm excitation, while Si-LPH film with 20 wt. % performs less well, due to a smaller absorbance caused by a lower LDH filler content (Figure 5a). Furthermore, the emission spectra of both Si-LPH films under excitation at 465 nm display a slight blue shift with respect to that of LDH powder

(Figure 5b). A blue shift is usually explained by a de-aggregation of phosphors, and the ratio between the monomer and excimer emission for silicone films is also changed, with a less distinct contribution of aggregates than for the powder. As expected, the shift is found to be more pronounced with a lower amount of LDH filler in the film. All these observations demonstrate that the production of the film provides an additional dilution effect to prevent TSP molecules from π-aggregating. However, this has no direct effect on the performance of PL QY_{abs} as it is counter-balanced by a smaller absorbance, dependent on the loading (Figure S8). Figure 5c shows a three-dimensional (3D) fluorescence plot of the emission intensity of Si-LPH film (40 wt.%) as a function of the excitation wavelength. This figure clearly shows that the film can be efficiently excited over a wide wavelength range.

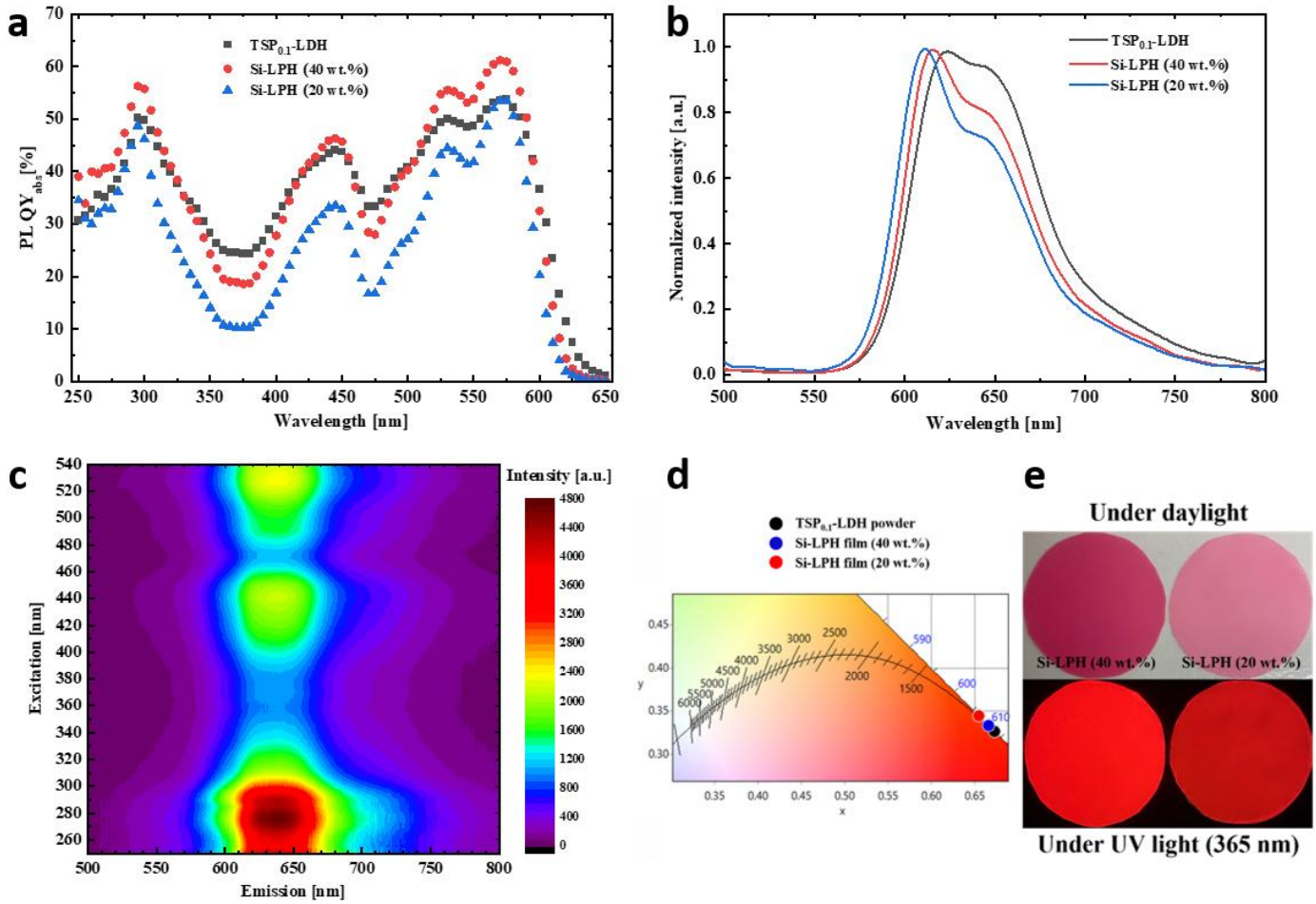

Figure 5. Evaluation of the composite films: Comparison between (a) PL QY_{abs} and (b) emission spectra of Si-LPH composite film (20 wt.%) (blue line), Si-LPH composite film (40 wt.%) (red line) and $TSP_{0.1}$-LDH powder (black line); (c) Three-dimensional (3D) luminescence plots of Si-LPH film (40 wt.%); (d) CIE chromaticity coordinates of TSP-LDH powder (black dot), Si-LPH (40 wt.%) (blue dot) and Si-LPH film (20 wt.%) (red dot); (e) photographs of Si-LPH film (40 wt.%) under daylight and 365 nm UV light.

The CIE color coordinates of $TSP_{0.1}$-LDH powder and both composite films display a saturated red color (Figure 5d), also

visible from photographs of the films when exposed to daylight or under UV at 365 nm (Figure 5e). This underlines that organo-modified LDH promotes the dispersion of the phosphor molecules in the silicone matrix, protects them from the external environment and renders them more robust and strongly emitting, thus making possible a combination with YAG in LED displays.

To apply this red phosphor to white LED solid-state lighting, it was combined with a commercial yellow YAG:Ce^{3+} phosphor excited at 465 nm with a commercial blue chip in remote configuration. Experimentally, the film stacking included Si-LPH film, Si-YAG film and a blue commercial chip, as shown in Figure 6. Different configurations were investigated and their associated emission spectra as well as CIE 1931 coordinates are presented.

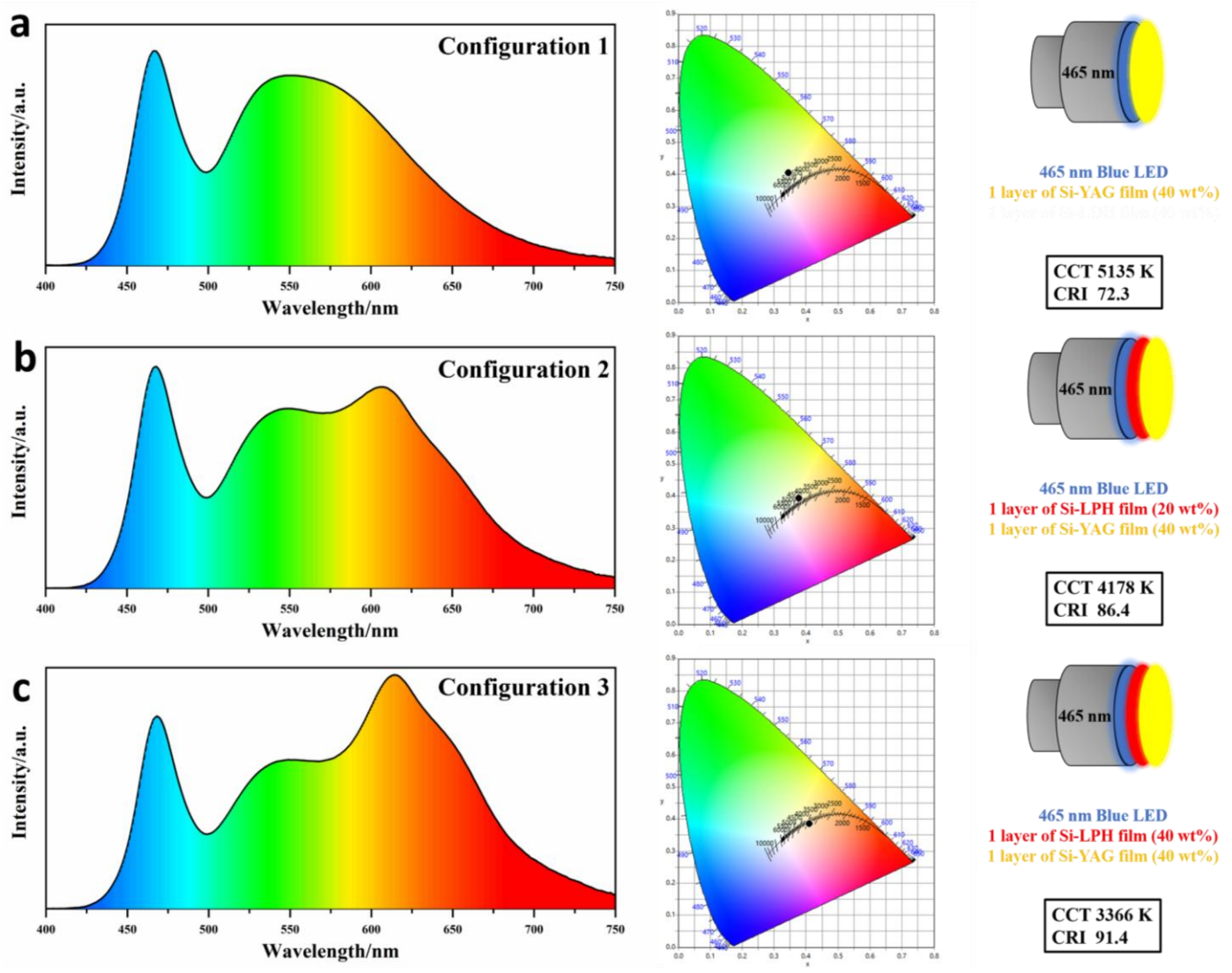

Figure 6. Emission spectra and photometric parameters of white LED prototypes designed using combinations of a commercial blue LED (465 nm) with (a) configuration 1: Si-YAG film, (b) configuration 2: Si-LPH film (20 wt.%) and Si-YAG film, (c) configuration 3: Si-LPH film (40

wt.%) and Si-YAG film.

For Si-YAG with a 465 nm LED itself, the color emission is greenish-yellow, thus producing a “cool white” light with CCT = 5135 K and CRI = 72.3. When the red-emitting Si-LPH (20 wt.%) composite film is located between the blue LED chip and the Si-YAG film, it contributes to “warming up” the white light produced, with CCT down to 4178 K and CRI up to 86.4. The position of CIE color coordinates is shifted towards the well-known blackbody curve. The stacking order has a significant effect on the photometric parameters; when reversed, the parameters lead to a warmer white light (Figure S9). This is due to the emission of the YAG film, which is not absorbed by the Si-LPH composite film, thus reducing its contribution while improving red emission. When the phosphor loading is higher, 40% instead of 20 wt. %, the red contribution is stronger in the overall spectrum (Fig. 5c). The optimal photometric parameters CT = 3366 K and CRI = 91.4 are reached; meanwhile, the position of the CIE color coordinates is on the blackbody curve, with a warm white obtained for the configuration LED/Si-LPH (40 wt.%)/Si-YAG.

In order to facilitate the implementation of the WLED prototype, another series of composite samples was fabricated by simultaneously dispersing together the two luminescent powders $TSP_{0.1}$-LDH and YAG:Ce^{3+} into one silicone film. Quantitatively, the composition of prepared Si-YAG-LPH composite film is 60 wt.% bi-component silicone matrix with 40 wt.% mixture of LDH and YAG phosphors, where the mass ratio between LDH and YAG ranges from 1:12 to 1:6 to tune its response at 465 nm excitation. The photometric parameters of configurations (4-6) are shown in Figure 7. As the mass ratio of LDH and YAG powder is 1: 12 (configuration 4), the CIE color coordinate is close to the blackbody curve. As expected, an increase in the relative quantity of LDH increases red emission and at the same time provides a warmer color temperature and a higher CRI. The latter configuration 1:6 leads to a CCT of 3409 K and a CRI of 88.6, comparable to configuration 3. Thus, this single Si-YAG-LPH composite film exhibits properties such as a broad and strong emission between 500 and 700 nm with optimized photometric parameters, relevant for warm white LED applications. Consequently, there is no significant re-absorption of the yellow emission arising from YAG:Ce phosphor by the red-emitting one, and this configuration based on a composite film alone can be considered more conducive to its implementation in WLED

prototypes.

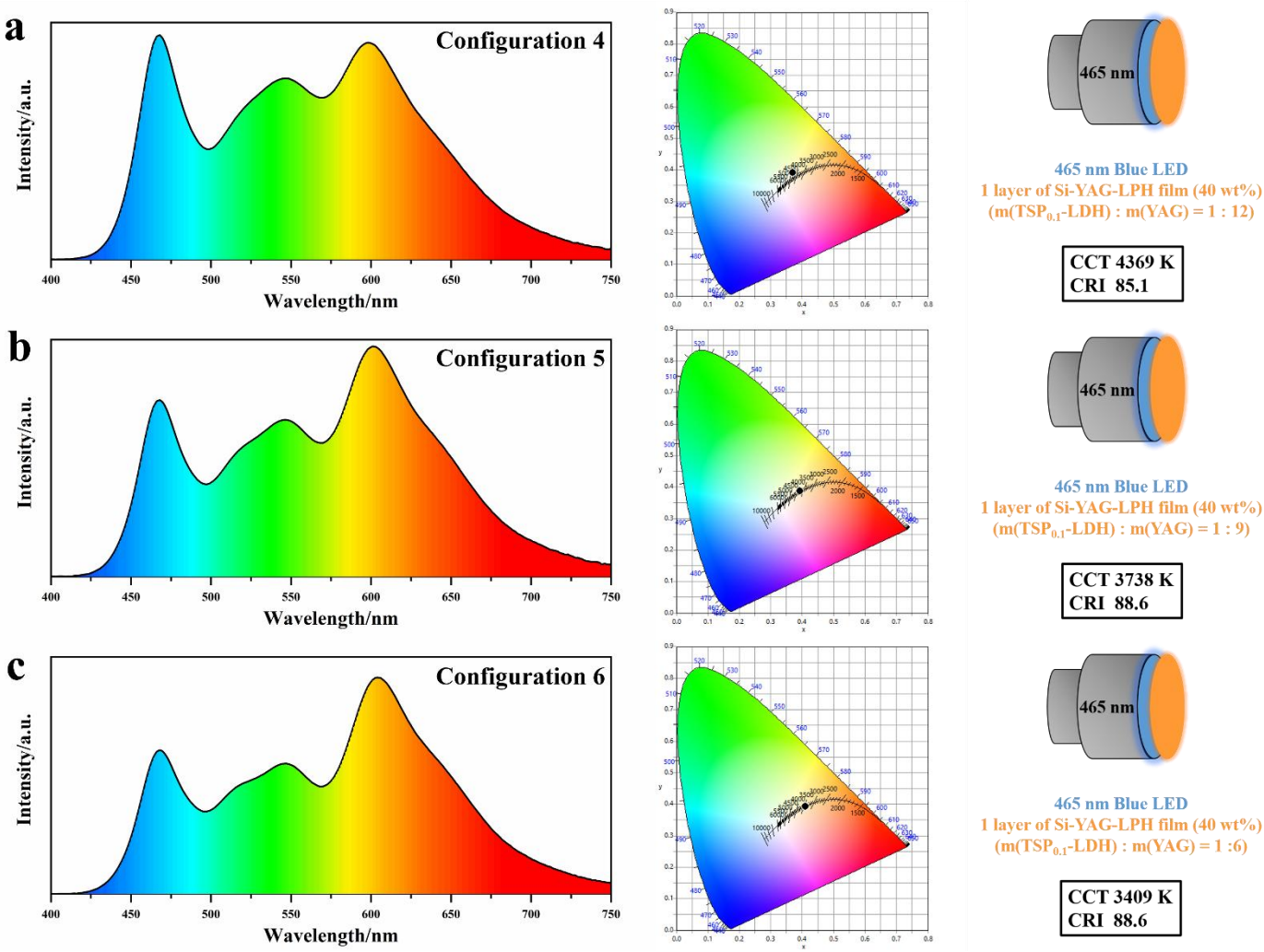

Figure 7. Emission spectra and photometric parameters of white LED prototypes implemented for configurations (a) 4, (b) 5, and (c) 6.

In order to assess the stability of TSP0.1-LDH powder and Si-LPH composite film in accelerated photonic conditions, both samples were irradiated by a powerful blue LED (460 nm, power: 2480 W/m^2) for 5000 minutes (about 84 hours) at 80°C or 120°C in a black chamber. A spectrophotometer recorded the emission spectra every 20 minutes for the entire duration. The variation in the integrated areas of the emission spectra as a function of irradiation time is illustrated in Figure 8. It should be stated that TSP molecules are highly thermally stable up to 400°C [46]. After a slight increase of the luminescence intensity, a plateau is quickly reached, whatever the sample considered. The powder and film being stable under photonic and thermal stress at 80°C after 5000 min, the temperature was increased to 120°C, in order to apply harsher conditions. Under these conditions, a significant drop in emission was recorded, with for example a 35% loss in 34 hours for the

powder. This unstable behavior under thermal radiation at 120°C is most probably due to the host structure composed of LDH sheets with spacer molecules. Indeed, hydroxyl inorganic LDH sheets as well as long alkyl chains of DS are known to be unstable under prolonged thermal treatment above 100°C. The strong dehydration of the former causes the loss of stacking and therefore indirectly the aggregation of the phosphors once they are no longer confined. [55]

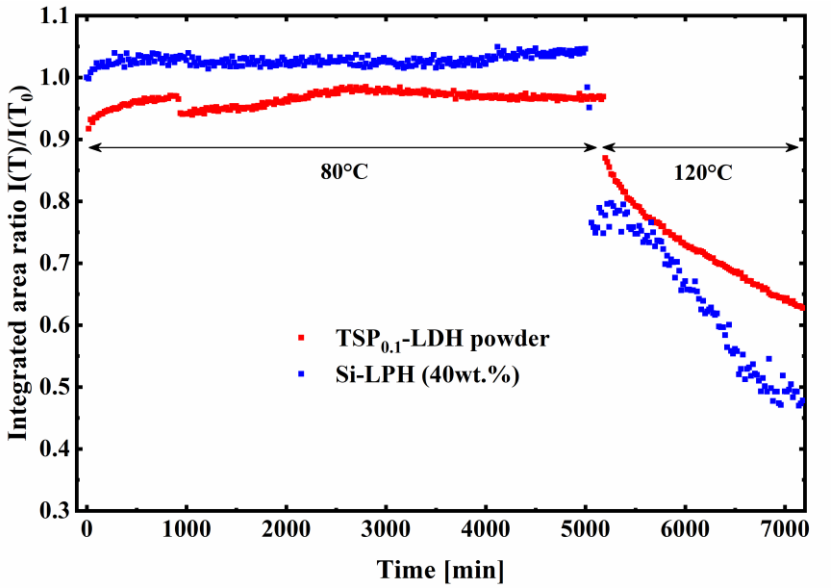

Figure 8. Variation in the integrated areas of the emission spectra as a function of irradiation time for TSP0.1-LDH powder (red plot) and for the Si-LPH (40 wt.%) film (blue plot) at 80°C for 5000 min and at 120°C until 7000 min.

More investigation is required to improve phosphor hybrid assembly stabilization in this higher temperature domain above 100°C. The emission spectra recorded after 3000 min (80°C) and 7000 min (120°C) of illumination by the blue LED illustrate this rapid drop in emission intensity for higher temperatures (Figure 9). We can note that the emission spectra recorded from the powder and the films annealed at 80°C are comparable to those recorded at room temperature. We can conclude that 120°C corresponds to a temperature limit after which the organic dyes and/or the LDH with spacers start to be affected.

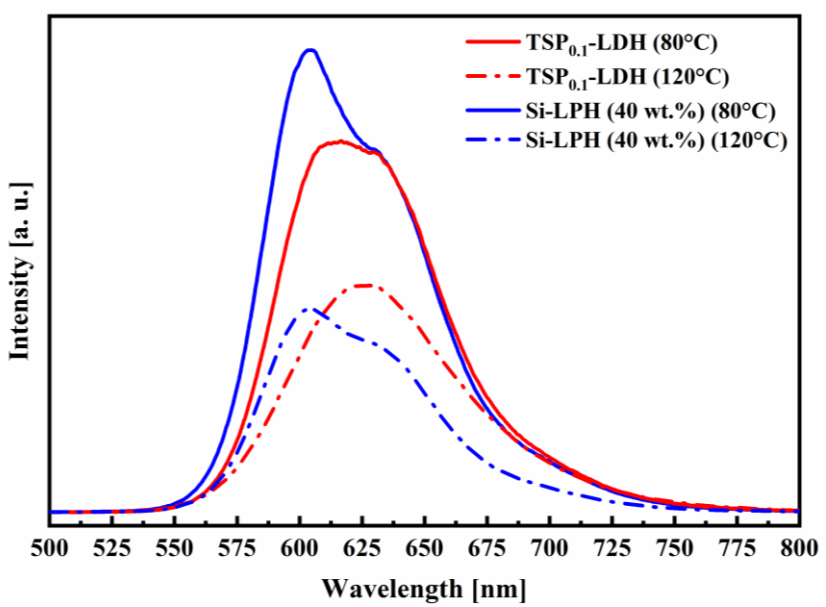

Figure 9. Emission spectra of powder (red curves) and film (blue curves) after 3000 min of ageing at 80°C (solid lines) and 7000 min of ageing at 120°C (dashed lines) under 460 nm LED irradiation.

These experiments show that these red phosphors (powder and film) can withstand combined photonic and thermal stresses to largely meet the requirements of LED devices.

3. Conclusion

The incorporation of (PDI)-based molecules bearing para-sulfonated aryls at the four bay positions (TSP) into a layered double hydroxide host is carried out successfully using a large amount of surfactant spacer. This guarantees the TSP molecules to be distant from each other, sufficiently to avoid aggregation-caused quenching, thus resulting in a high quantum yield for the phosphors from within the hybrid host. This contrasts drastically with TSP, which does not emit in its solid state due to the intermolecular distance of about 1.2 nm, which is not sufficient to cancel the aggregation phenomenon and consequently the extinction of the emission light. When co-hosted in LDH with a surfactant in tiny quantities, an absolute photoluminescence quantum yield of about 35 % is reached upon blue excitation at 465 nm for a dye content as low as 0.1 % of the total interleaved anions, characterized by an emission band centered at 655 nm. This rare-earth free red phosphor combined with a yellow phosphor and a blue LED resulted in warm white light with a CRI above 90 in remote phosphor configuration by using silicone as an encapsulant. The appropriate stability of the system under combined photonic and thermal stress confirms the interest of the TSP-LDH material as a red phosphor in blue LED-based lighting

and/or display devices.

4. Experimental section

4.1. Chemicals

All the reagents were purchased from commercial sources and used without further purification. 1,6,7,8-tetrachloroperylene-3,4,9,10-tetracarboxylic acid dianhydride (PTCD-4Cl, 96%) was obtained from Aladdin. Propionic acid (99%), phenol (99%), dichloromethane (DCM, 99%), 2,6-diisopropylaniline (97%), and *N*-methylpyrrolidone (NMP, 99%) were provided by Acros Organics. Magnesium nitrate hexahydrate ($Mg(NO_3)_2 \cdot 6H_2O$, 99.9%), aluminum nitrate nonahydrate ($Al(NO_3)_3 \cdot 9H_2O$, 99.9%), sodium hydroxide (NaOH, 97%), sodium dodecylsulfate ($CH_3(CH_2)_{11}SO_4Na$, 98.5%), concentrated sulfuric acid (H_2SO_4, 98%), anhydrous potassium carbonate (K_2CO_3, 99.9%), and concentrated hydrochloric acid (HCl, 37%) were purchased from Sigma-Aldrich. Additionally, YAG:Ce^{3+} phosphor and the two-component silicone polymer, Bluesil™ RTV 141 A&B, were supplied respectively by Phosphortech and Bluestar Silicones (now Elkem).

4.2. Synthesis of *N*,*N*′-bis(2,6-diisopropylphenyl)-1,6,7,12-tetra-[4-(sulfuric acid)phenoxy]perylene-3,4,9,10-tetracarboxydiimide (TSP)

The synthesis of TSP was performed adapting reported literature procedures [15] as indicated in the Supporting Information via a three-step process (Figure 10).

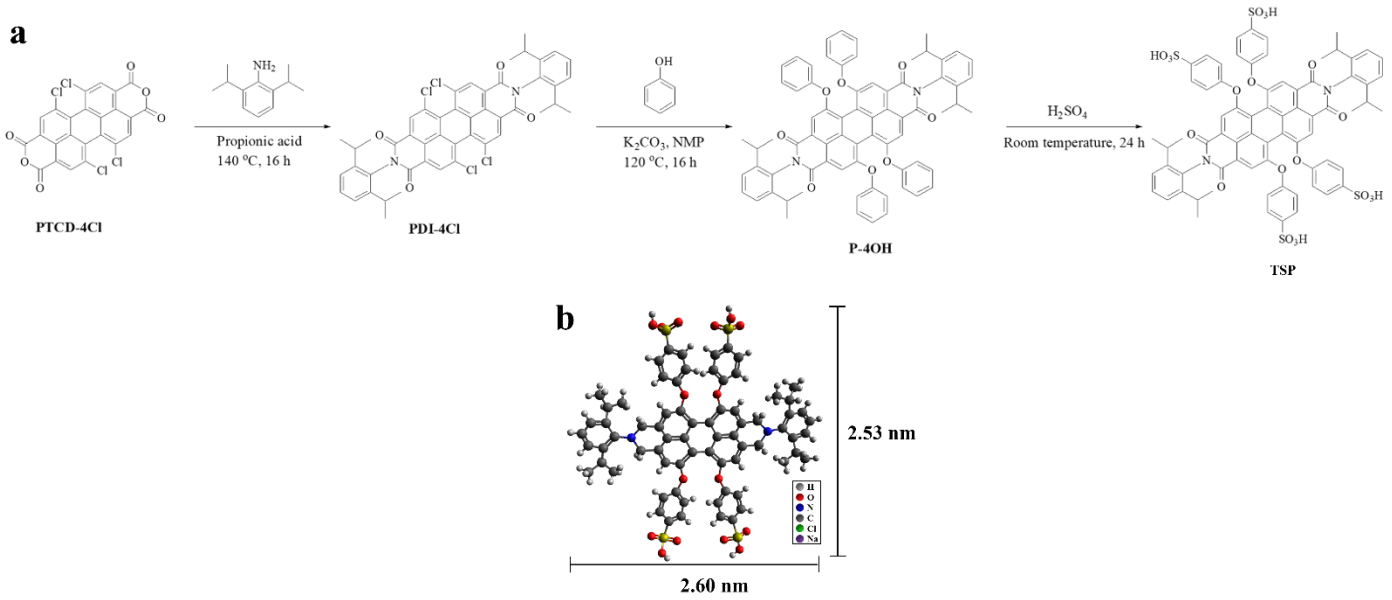

Figure 10. (a) Synthetic route to prepare TSP and (b) its schematic representation in 3D computed using Avogadro

4.3. Synthesis of TSP_x-LDH nanofillers

TSP and sodium dodecyl sulfonate (SDS) were co-intercalated into the interlayer galleries of LDH by a co-precipitation step leading to the series of organo-modified samples $DS_{1-x}TSP_x$-LDH (marked by TSP_x-LDH). Experimentally, 0.51 g of $Mg(NO_3)_2 \cdot 6H_2O$ (2 mmol) and 0.38 g of $Al(NO_3)_3 \cdot 9H_2O$ (1 mmol) were dissolved in 50 mL of deionized water to form solution A, 0.24 g of NaOH (6 mmol) was dissolved in 50 mL of deionized water as B, and C was composed of 50 mL of aqueous solution containing SDS (a mmol) and TSP (b mmol), its relative value x was related to the feeding molar ratio between SDS and TSP as x (%) = b/(a + b) × 100 (%) with a + 4b = n (Al^{3+}), x ranging from 0.005 to 1. Solution A was added dropwise to solution C at a rate of 0.4 mL/min at room temperature under nitrogen, and the pH of the blended solution was maintained at 9.5-10 using solution B. The mixture was then stirred overnight at room temperature under N_2. A final pinkish-purple slurry was centrifuged and washed several times with deionized water, and then dried at 40°C for 24 h.

4.4. Fabrication of silicone/TSP_x-LDH composite films

The two-component silicone polymer (Bluesil^{TM} RTV 141 A&B) was composed of a viscous liquid (part A, 90 wt.%), cured by a polyaddition reaction with a catalyst (part B, 10 wt.%). A varying quantity of TSP_x-LDH powders was mixed into the silicone. For example, a 40 wt.% load was prepared by mixing, at 1200 rpm for 10 min, 1.62 g of part A with 1.2 g of $TSP_{0.1}$-LDH using a mechanical mixer (“Thinky Mixer” Planetary Centrifugal Vacuum Mixer). The mixture was further

homogenized by passing it twice through a three-roller mill (Exakt80E). 0.18 g of part B was added to the mixture and homogenized using the mechanical mixer for 10 min at 1200 rpm. Finally, the silicone/$TSP_{0.1}$-LDH film (labelled Si-LPH film (40 wt.%)) was cast on a Teflon surface (Elcometer 4340 automatic film applicator) at 40°C, with a knife blade height of 200 μm and a casting speed of 30 mm/s, then cured at 70°C for another 2 h. The film thickness was measured using an Elcometer 456 coating thickness gauge and all the values were in the range 120 ± 5 μm. Silicone/$TSP_{0.1}$-LDH film with loading rates of 20 wt.% (called Si-LPH film (20 wt.%)), silicone/YAG:Ce^{3+} (marked Si-YAG film) and silicone/YAG-$TSP_{0.1}$-LDH (tagged Si-YAG-LPH film) film were prepared similarly, with the Si-YAG film loaded with 40 wt.% commercial YAG:Ce^{3+} powder, and the Si-YAG-LPH film prepared with 40 wt.% of the mixture of YAG : Ce^{3+} and $TSP_{0.1}$-LDH powders.

4.5. Characterization

Powder X-ray diffraction (PXRD) patterns of TSP_x-LDH powders and silicone/LDH films were obtained using a Philips X-Pert Pro diffractometer with Cu Kα radiation (λ = 0.154 nm) in the range of 2-70°/2θ with a step size of 1°/min. Fourier transform infrared (FT-IR) spectra in the range from 4000 to 400 cm^{-1} with a summation of 64 scans and 2 cm^{-1} resolution were recorded on a Thermo-Nicolet 5700 FT-IR spectrometer using the KBr pellet technique with a sample/KBr ratio of 1:100. ^1H NMR spectra were collected in Fourier Transform mode with a Bruker AVANCE 400 at 400 MHz and 298K using DMSO as the solvent. Ultraviolet-visible (UV-vis) absorption spectra of samples were measured using a Shimadzu UV-2600 spectrophotometer in the range of 200-800 nm. The film microstructure was observed using a Zeiss Supra 55 scanning electron microscope operating at 3 kV (SEM and EDX analysis). The internal photoluminescence quantum yield ($PL\ QY_{int}$), absorption coefficient (Abs.), emission spectra (EM), and trichromatic coordinates (CIE x,y) were recorded with PL QY measurement software (U6039-05) using an integrating sphere measurement system (C9920-02G) from Hamamatsu Photonics. The setup was composed of a 150 W monochromatized Xenon lamp, an integrating sphere (Spectralon coating, diameter =3.3 inch), and a high-sensitivity CCD camera. Photometric parameters were collected in an integrating sphere with a diode array rapid analyzer system (GL Optic GLS 500 integrating sphere) at room temperature. Si-LPH, Si-YAG, and

Si-YAG-LPH films were placed on a blue LED emitting at 465 nm. Testing conditions included a forward current of 450 mA related to an applied voltage of 3.2 V. Reliability studies were carried out using a home-made setup consisting of a power-controlled blue LED emitting at 460 nm as the excitation source and a HR4000 high resolution spectrometer (Ocean Optics) as the PL analyser. Samples were positioned on a heating element whose temperature was adjusted to the desired value (80°C or 120°C). The emission spectra of the samples were acquired every 20 min for several hours. Their area was integrated to obtain the total emission intensity. LED power was measured using a Scientech Mentor MA 10 model with a MC2501 calorimetric head unit (25.4 mm aperture). The measurement was performed by centering the head unit over the LED source and measuring the power of the LED light emitted through the aperture. The blue LED power was 183 mW. LED power density can be expressed in W/m^2 and was calculated by LED power (in watt) per unit surface of the sample (0.25 cm^2). The power density of the blue LED was 9300 W/m^2; for our experiments, a filter was used in order to reduce this value to 2480 W/m^2.

Acknowledgments

Y. Guo gratefully acknowledges the financial support from the Joint Funds of the National Natural Science Foundation of China (Grant No. ZK20180055) and Programs for Foreign Talent (No. G2021106012L). Also, Y. Guo thanks the financial support from China Scholarship Council (No. 202006880036).

References

1. X. Zhang, W. Liu, G. Z. Wei, D. Banerjee, Z. Hu, J. Li, *J. Am. Chem. Soc*. 2014, **136**, 14230.
2. Z. Xia, Z. Xu, M. Chen, Q. Liu, *Dalton Trans*. 2016, **45**, 11214.
3. J. McKittrick, L.E. Shea-Rohwer, *J. Am. Ceram. Soc*. 2014, **97**, 1327.
4. Z. Wang, Z. Yang, N. Wang, Q. Zhou, J. Zhou, L. Ma, X. Wang, Y. Xu, M. G. Brik, M. D. Dramic'anin, M. Wu, *Adv. Opt. Mater*. 2020, **8**, 1901512.
5. Y. Chen, J. Chen, J. Liang, J. He, Z. Liu, Y. Yin, *Chem. Mater*. 2020, **32**, 9551.
6. Y. Wei, H. Yang, Z. Gao, Y. Liu, G. Xing, P. Dang, A. A. Al Kheraif, G. Li, J. Lin, R. Liu, *Adv. Sci*. 2020, **7**, 1903060.
7. Y. Hu, W. Zhuang, H. Ye, S. Zhang, Y. Fang, X. Huang, *J. Lumin*. 2005, **111**, 139.
8. C. C. Lin, A. Meijerink, R.-S. Liu, *J. Phys. Chem. Lett*. 2016, **7**, 495.
9. R. Verstraete, H. F. Sijbom, J. J. Joos, K. Korthout, D. Poelman, C. Detavernier, P. F. Smet, A*CS Appl. Mater. Interfaces* 2018, **10**, 18845.

10. F. Würthner, C. R. Saha-Möller, B. Fimmel, S. Ogi, P. Leowanawat, D. Schmidt, *Chem. Rev*. 2015, **116**, 962.
11. S. Chen, P. Slattum, C. Wang, L. Zang, *Chem. Rev*. 2015, **115**, 11967.
12. A. Nowak-Król, F. Würthner, *Org. Chem. Front*. 2019, **6**, 1272.
13. F. Würthner, *Chem. Commun*. 2004, **35**, 1564.
14. X. Zhan, A. Facchetti, S. Barlow, T. J. Marks, M. A. Ratner, M. R. Wasielewski, S. R. Marder, *Adv. Mater*. 2011, **23**, 268.
15. C. Kohl, T. Weil, J. Qu, K. Müllen, *Chem. Eur. J*. 2004, **10**, 5297.
16. F. Ito, Y. Kogasaka, K. Yamamoto, *J. Phys. Chem. B* 2013, **117**, 3675.
17. B. Zhang, H. Soleimaninejad, D. J. Jones, J. M. White, K. P. Ghiggino, T. A. Smith, W. W. H. Wong, *Chem. Mater*. 2017, **29**, 8395.
18. L. Zong, Y. Gong, Y. Yu, Y. Xie, G. Xie, Q. Peng, Q. Li, Z. Li, *Sci. Bull*. 2018, **63**, 108.
19. D. Schmidt, M. Stolte, J. Sgß, A. Liess, V. Stepanenko, F. Wgrthner, *Angew. Chem*. 2019, **131**, 13519.
20. L. Zong, H. Zhang, Y. Li, Y. Gong, D. Li, J. Wang, Z. Wang, Y. Xie, M. Han, Q. Peng, X. Li, J. Dong, J. Qian, Q. Li, Z. Li, *ACS Nano* 2018, **12**, 9532.
21. M. Stolte, T. Schembri, J. Süß, D. Schmidt, A.-M. Krause, M. O. Vysotsky, F. Würthner, *Chem. Mater*. 2020, **32**, 6222.
22. A. F. Coleman, M. Chen, J. Zhou, J. Y. Shin, Y. Wu, R. M. Young, M. R. Wasielewski, *J. Phys. Chem. C* 2020, **124**, 10408.
23. C. W. Struijk, A. B. Sieval, J. E. J. Dakhorst, M. Dijk, P. Kimkes, R. B. M. Koehorst, H. Donker, T. J. Schaafsma, S. J. Picken, A. M. Craats, J. M. Warman, H. Zuilhof, E. J. R. Sudhölter, *J. Am. Chem. Soc*. 2000, **122**, 11057.
24. T. Vosch, J. Hofkens, M. Cotlet, F. Köhn, H. Fujiwara, R. Gronheid, K. V. D. Biest, T. Weil, A. Herrmann, K. Müllen, S. Mukamel, M. V. Auweraer, F. C. D. Schryver, *Angew. Chem*. 2001, **113**, 4779.
25. M. Golshan, E. Rostami-Tapeh-Esmail, M. Salami-Kalajahi, H. Roghani-Mamaqani, *Eur. Polym. J*. 2020, **137**, 109933.
26. J. Sun, S. Zou, Z. Wang, X. Zhang, J. Shen, *Mater. Sci. Eng. C* 1999, **10**, 123.
27. R. O. Marcon, S. Brochsztain, *J. Phys. Chem. A* 2009, **113**, 1747.
28. J. Li, S. Yuan, J.-S. Qin, L. Huang, R. Bose, J. Pang, P. Zhang, Z. Xiao, K. Tan, A. V. Malko, T. Cagin, H.-C. Zhou, *ACS Appl. Mater. Interfaces* 2020, **12**, 26727.
29. S. Wu, D. Ren, K. Zhou, H.-L. Xia, X.-Y. Liu, X. Wang, J. Li, *J. Am. Chem. Soc*. 2021, **143**, 10547.
30. B. Lü, Y. Chen, P. Li, B. Wang, K. Müllen, M. Yin, *Nat. Commun*. 2019, **10**, 767.
31. C. Chakraborty, K. Dana, S. Malik, *J. Phys. Chem. C* 2011, **115**, 1996.
32. J. Bauer, P. Behrens, M. Speckbacher, H. Langhals, *Adv. Funct. Mater*. 2003, **13**, 241.
33. R. Gao, M. S. Kodaimatic, D. Yan, *Chem. Soc. Rev*. 2021, **50**, 5564.
34. S. Li, J. Lu, M. Wei, D. G. Evans, X. Duan, *Adv. Funct. Mater*. 2010, **20**, 2848.
35. C. Li, R. Liang, R. Tian, S. Guan, D. Yan,.J. Luo, M. Wei, D. G. Evans, X. Duan, *RSC Adv*. 2016, **6**, 16608.
36. P. Legentil, F. Leroux, S. Therias, D. Boyer, G. Chadeyron, *J. Mater. Chem. C* 2020, **8**, 11906.
37. J. Yu, Q. Wang, D. O'Hare, L. Sun, *Chem. Soc. Rev*. 2017, **46**, 5950.
38. C. Jing, B. Dong, Y. Zhang, *Energy Environ. Mater*. 2020, **3**, 346.
39. C. Taviot-Guého, V. Prévot, C. Forano, G. Renaudin, C. Mousty, F. Leroux, *Adv. Funct. Mater*. 2017, **28**, 1703868.
40. P. Gu, S. Zhang, X. Li, X. Wang, T. Wen, R. Jehan, A. Alsaedi, T. Hayat, X. Wang, *Environ. Pollut*. 2018, **240**, 493.
41. R. Valleix, Q. Zhang, D. Boyer, P. Boutinaud, G. Chadeyron, Y. Feng, H. Okuno, F. Réveret, H. Hintze-Bruening, F. Leroux, *Adv. Mater*. 2021, **38**, 2103411.
42. R. Ma, R. Li, X. Liu, P. Zhang, X. Yang, J. Lu, *Adv. Optical Mater*. 2020, **8**, 1902019.
43. D. Gçrl, X. Zhang, F. Wrthner, *Angew. Chem. Int. Ed*. 2012, **51**, 6328.
44. M. Sun, K. Müllenb, M. Yin, *Chem. Soc. Rev*. 2016, **45**, 1513.
45. H. Jang, J. W. Namgoong, M.-G. Sung, Y. Chang, J. P. Kima, *Dyes Pigm*. 2018, **158**, 142.
46. S. Choi, K. H. Cho, J. W. Namgoong, J. Y. Kim, E. S. Yoo, W. Lee, J. W. Jung, J. Choi, *Dyes Pigm*. 2019, **163**, 381.

47. P. E. Hartnett, S. M. Dyar, E. A. Margulies, L. E. Shoer, A. W. Cook, S. W. Eaton, T. J. Marks, M. R. Wasielewski, *Chem*. *Sci*. 2015, **6**, 402-411.
48. V. Grande, B. Soberats, S. Herbst, V. Stepanenkoa, F. Würthner, *Chem*. *Sci*. 2018, **9**, 6904.
49. Y.-L. Wu, N. E. Horwitz, K.-S. Chen, D. A. Gomez-Gualdron, N. S. Luu, L. Ma, T. C. Wang, M. C. Hersam, J. T. Hupp, O. K. Farha, R. Q. Snurr, M. R. Wasielewski, *Nat*. *Chem*. 2017, **9**, 466.
50. B. Lü, P. Li, P. Li, Y. Zhang, K. Müllen, M. Yin, *J*. *Mater*. *Chem*. *C*, 2020, **8**, 1421.
51. S. Li, J. Lu, H. Ma, J. Xu, D. Yan, M. Wei, D. G. Evans, X. Duan, *Langmuir* 2011, **27**, 11501.
52. S. Li, J. Lu, H. Ma, D. Yan, Z. Li, S. Qin, D. G. Evans, X. Duan, *J*. *Phys*. *Chem*. *C* 2012, **116**, 12836.
53. S. Yagai, T. Seki, T. Karatsu, A. Kitamura, F. Würthner, *Angew*. *Chem*. *Int*. *Ed*. 2008, **47**, 3367.
54. C. Chakraborty, K. Dana, S. Malik, *J*. *Phys*. *Chem*. *C* 2012, **116**, 21116.
55. P. Legentil, F. Leroux, S. Therias, D. Boyer, F. Reveret, G. Chadeyron, *Appl. Clay Sci.* 2021, **201**, 105922.